

Supramolecular Birefringent Metallogels formed by Trinuclear Copper(II) complexes with myo-inositol and bipyridyl ligands

Aditya A. Puranik, Priyanka S. Salunke, Neelima D. Kulkarni*

*Department of Chemistry, Faculty of Science,

The Maharaja Sayajirao, University of Baroda, Vadodara, 390002 Gujarat, India.

E-mail: nk_msu@yahoo.co.in, ndkulkarni-chem@msubaroda.ac.in ; Tel: +91(265)2795552

Supplementary Information

- | | | |
|----|---|-----------------------|
| a) | Figure S1¹H NMR spectrum of inositol | page no:2 |
| b) | Figure S2-S8: ESI-MS of metallogels | page no:2-5 |
| c) | Figures S9-S14: IR analysis of Xerogels | page no: 5-8 |
| d) | Thermal analysis | |
| 1) | Figure S15-S19: TG-DTA analysis of gels | page no: 9-11 |
| 2) | Figure S20-S24: TG-DTA analysis of Xerogels | page no: 12-14 |
| e) | Figure S25: Effect of anions in the formation | page no:-14 |
| f) | Figures S26-S27: Rheological studies of metallogels | page no -15 |
| g) | Figure S28: Polarized microscope images (POM) | page no -16 |
| h) | Table TS1.: Optimized geometrical parameters involving metal coordination. | page no - 17 |

a) ^1H NMR spectrum of inositol

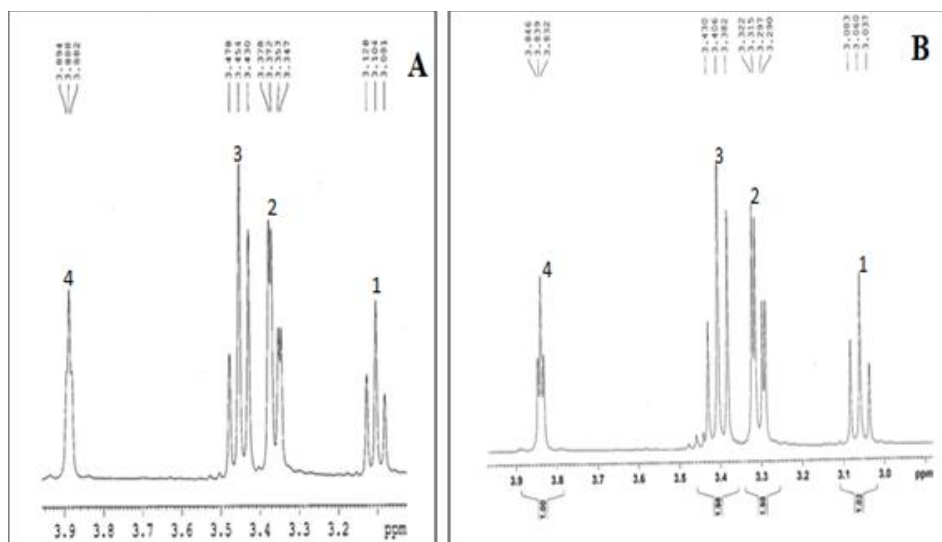


Figure S1: Figure 3. [A] ^1H NMR spectrum of inositol and [B] ^1H NMR spectrum of inositol+base (KOH).

b) ESI-MS of metallogels

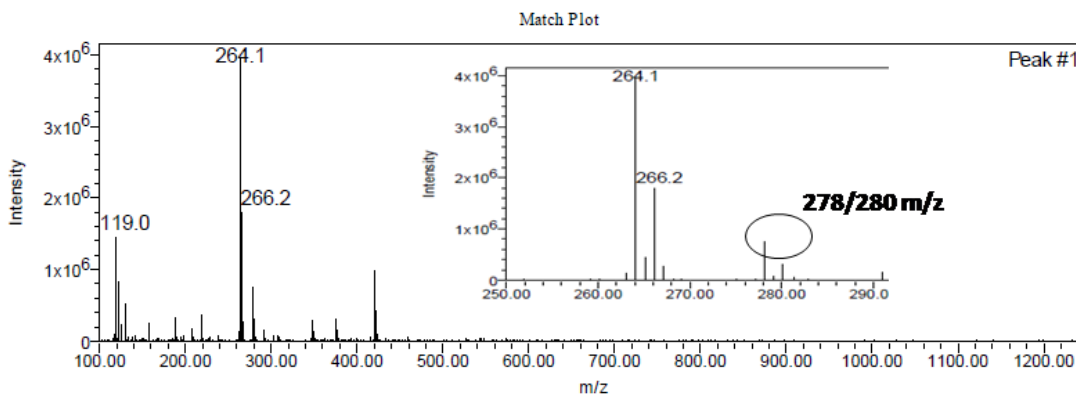


Figure S2. ESI-MS of the metallogel-111.

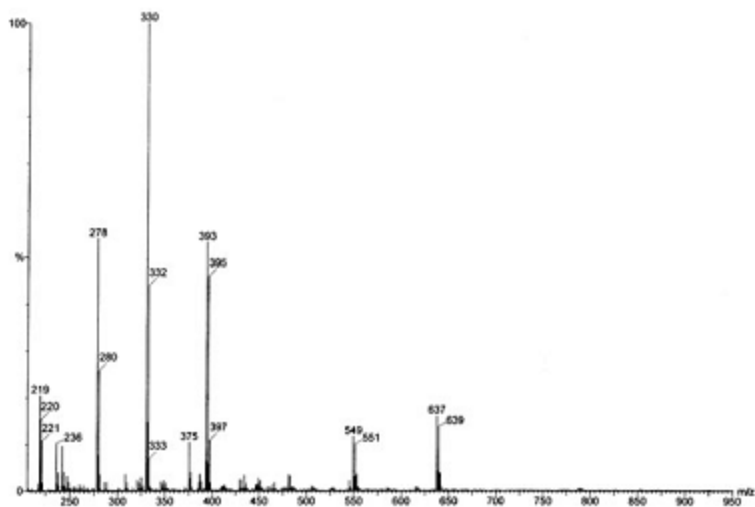


Figure S3. ESI-MS of the metallogel-112.

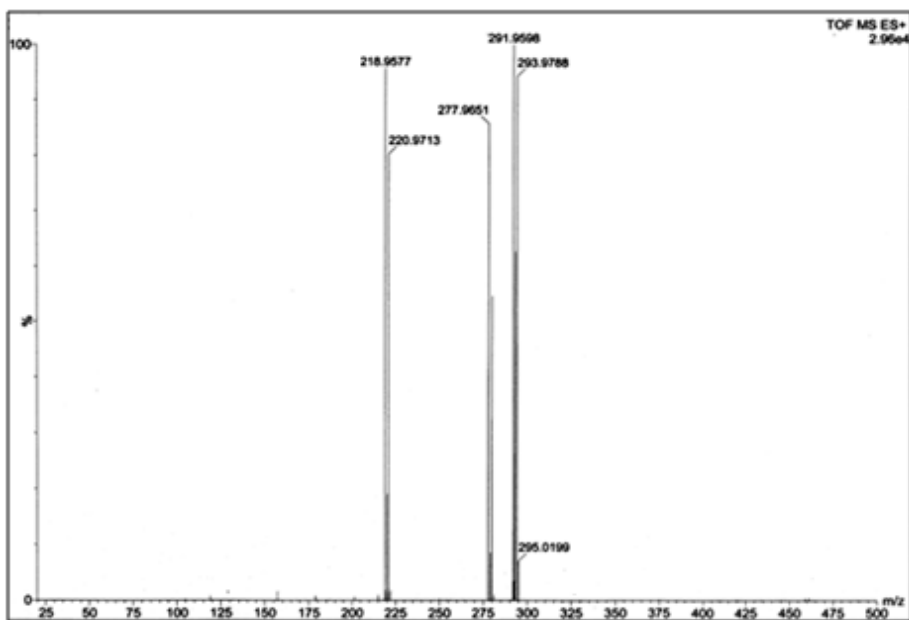


Figure S4. ESI-MS of the hydrogel 113.

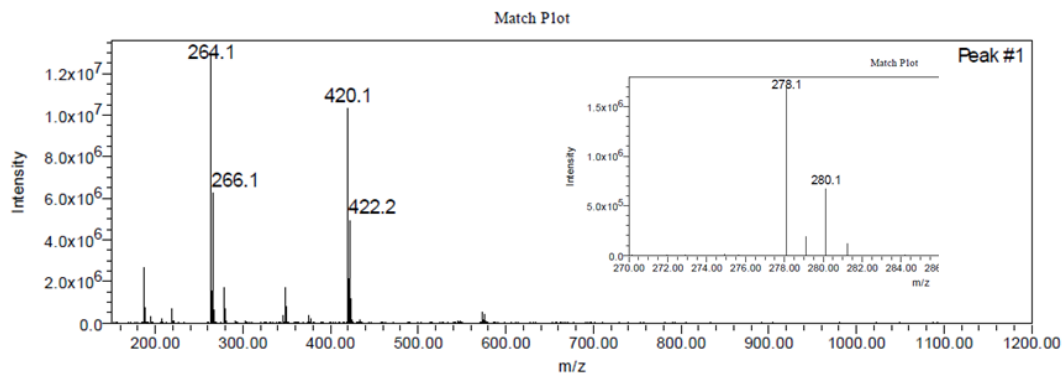


Figure S5. ESI-MS of the metallogel-121.

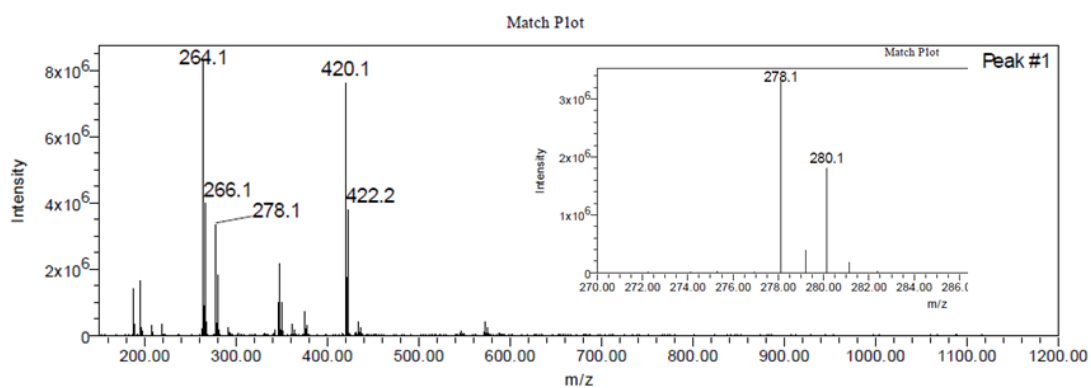


Figure S6. ESI-MS of the metallogel-122.

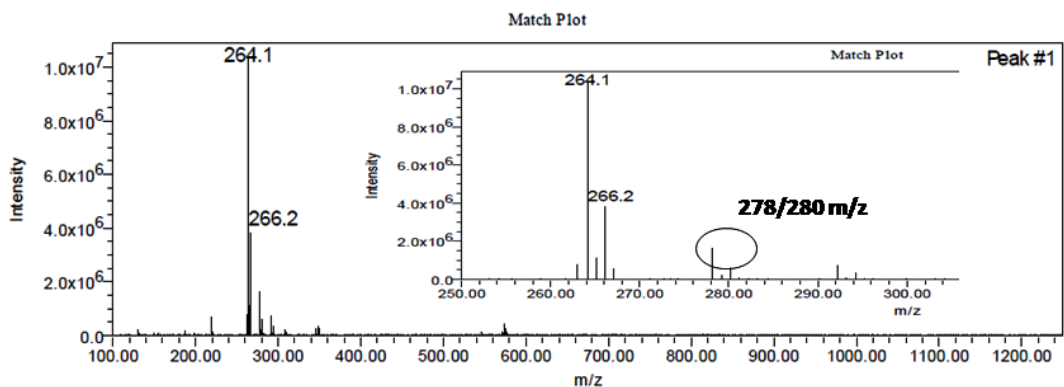


Figure S7. ESI-MS of the metallogel-123.

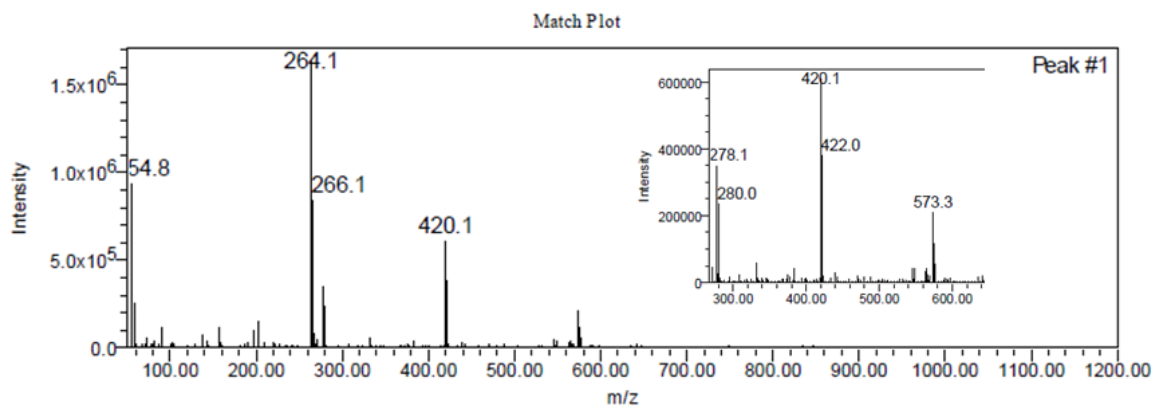


Figure S8. ESI-MS of the metallogel-114.

c) IR analysis of Xerogels

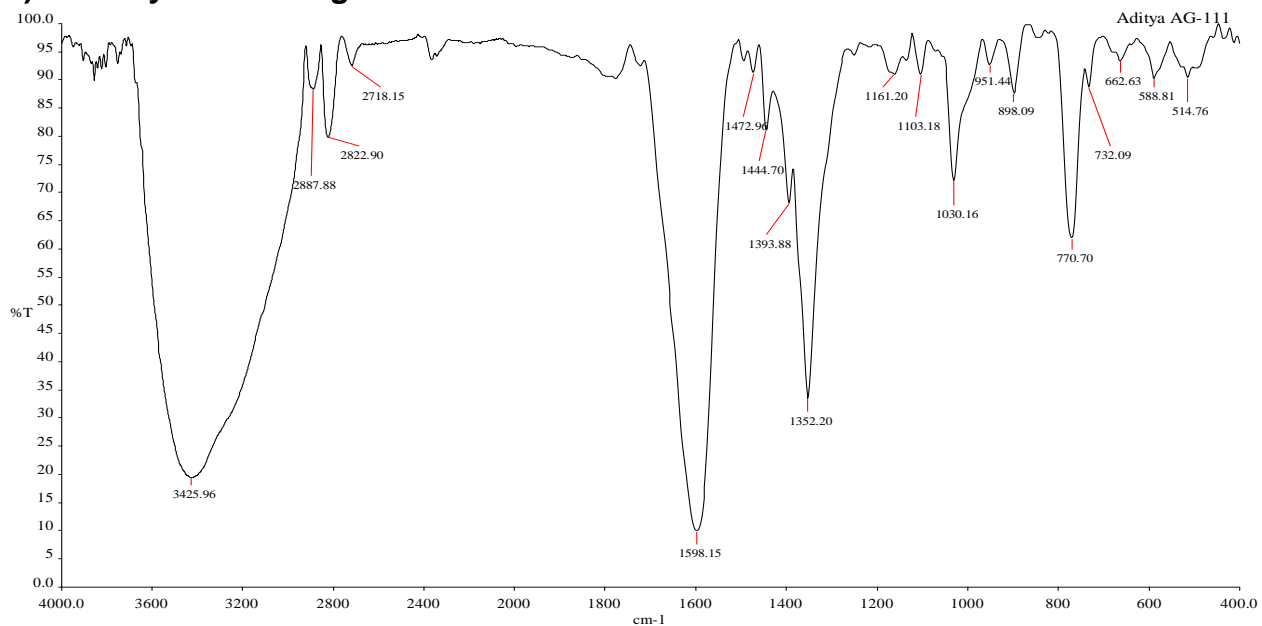


Figure S9. IR spectrum of gel 111.

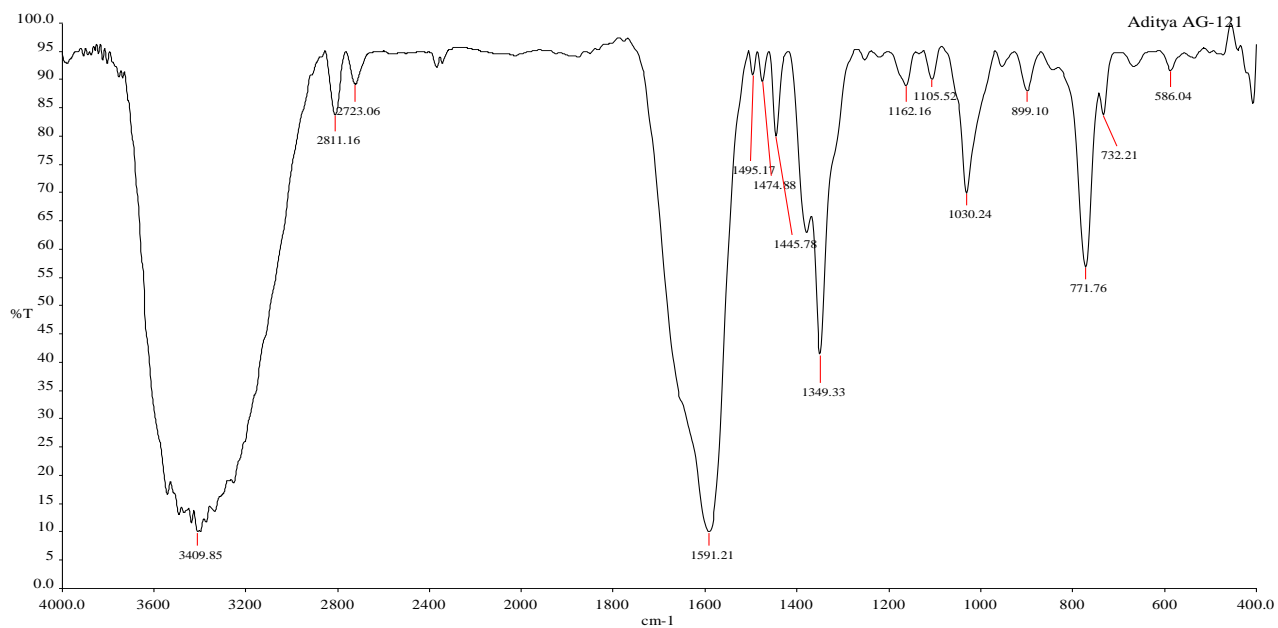


Figure S10. IR spectrum of gel 121.

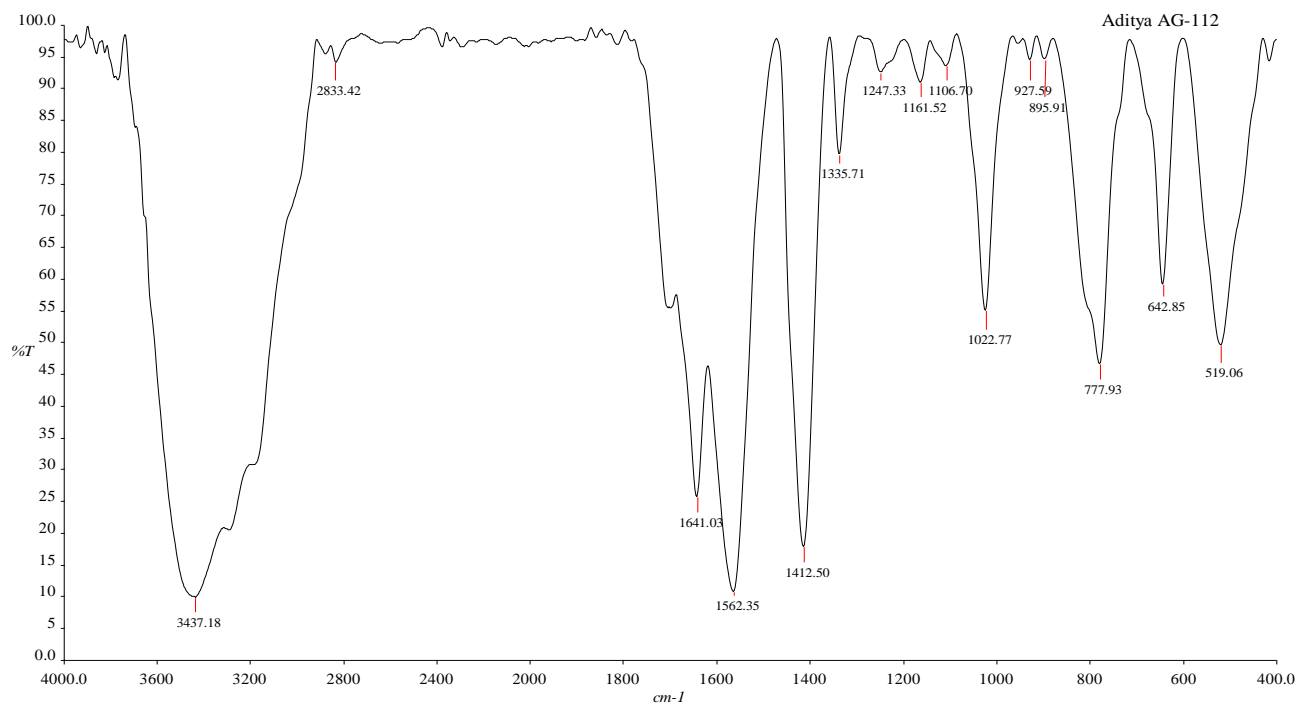


Figure S11. IR spectrum of gel 112.

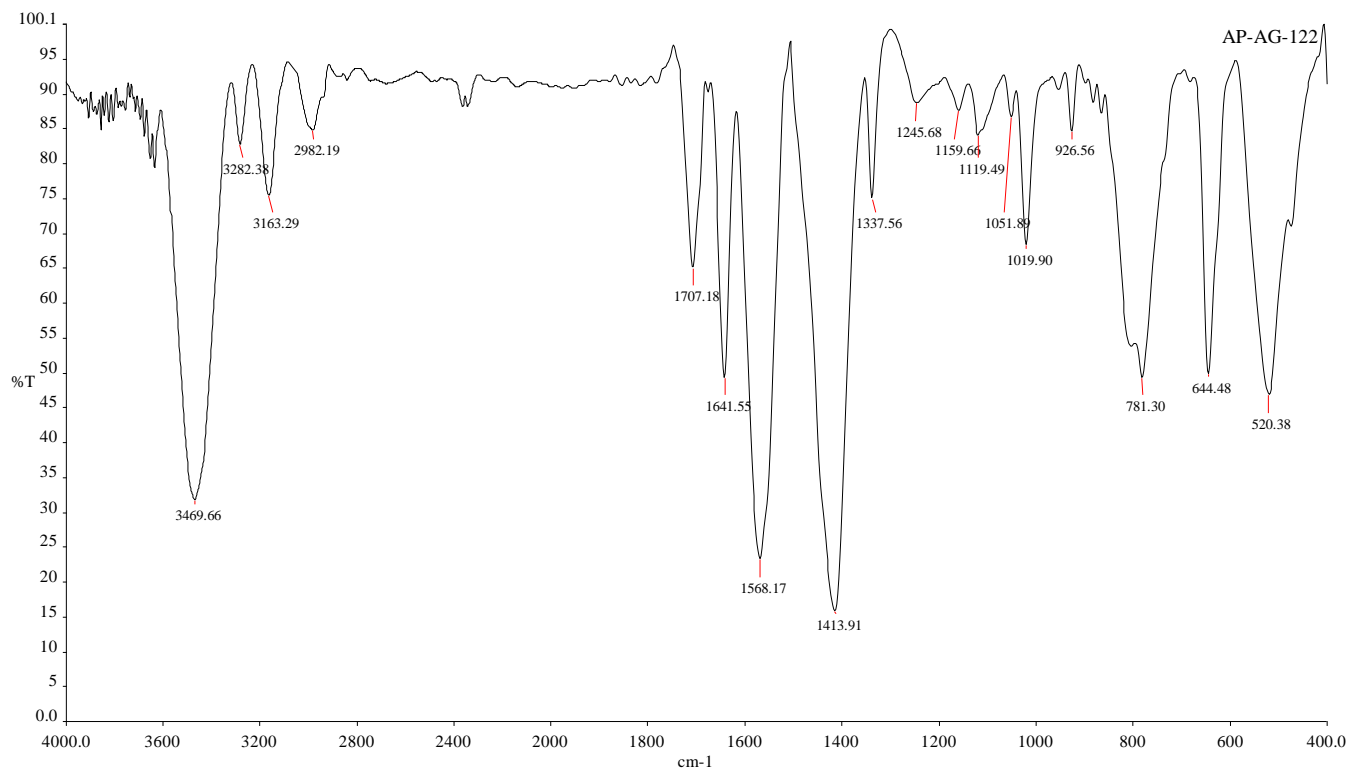


Figure S12. IR spectrum of gel 122.

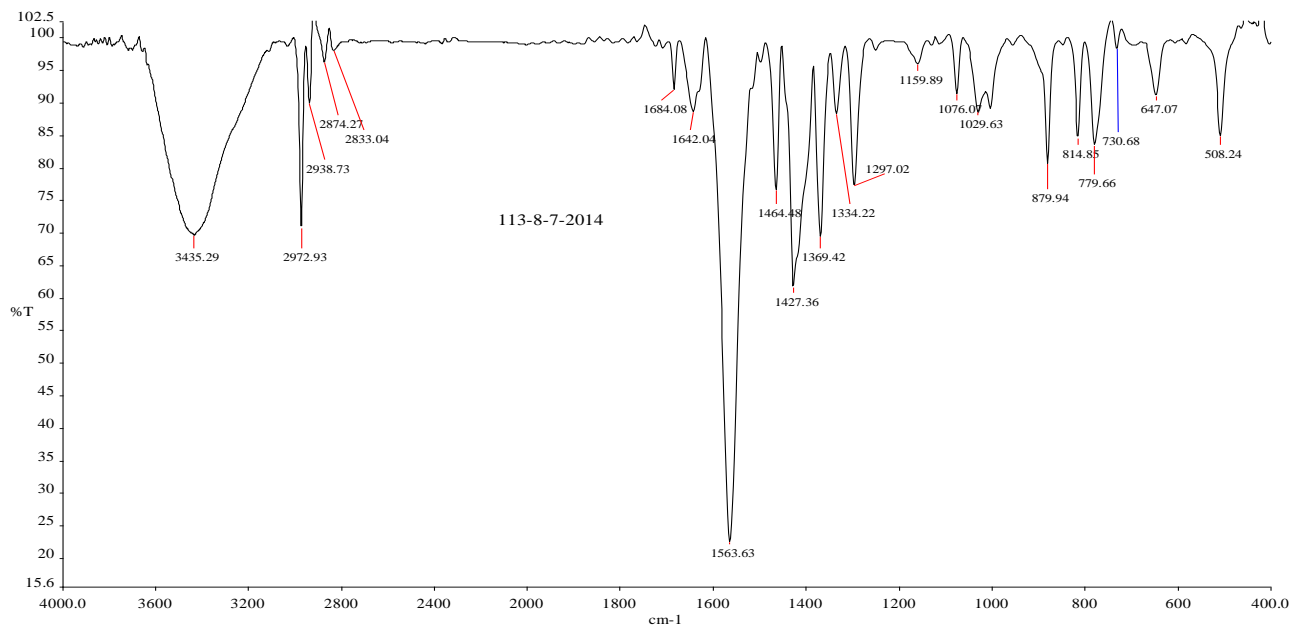


Figure S13. IR spectrum of gel 113.

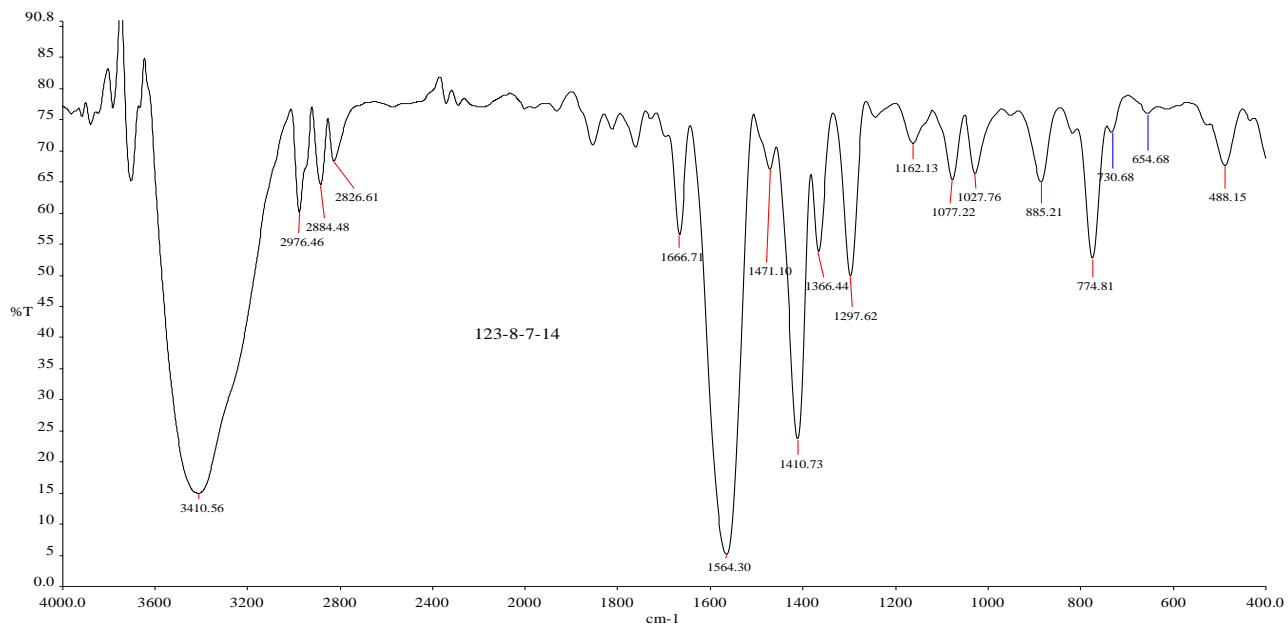


Figure S14. IR spectrum of gel 123.

d) Thermal analysis

TG- DTA of gels

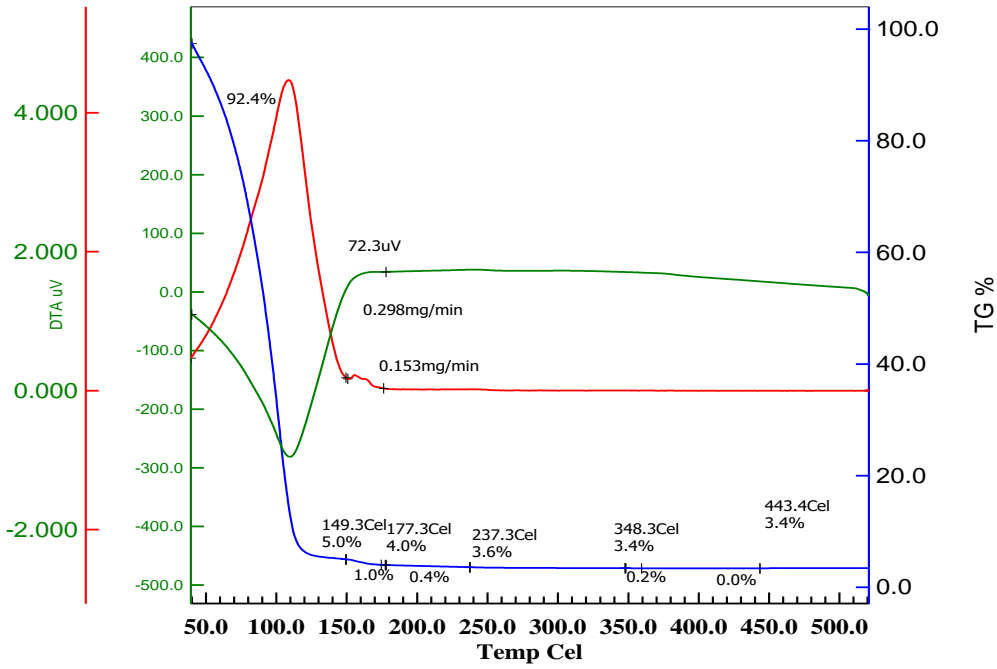


Figure S15: TG-DTA of gel 111

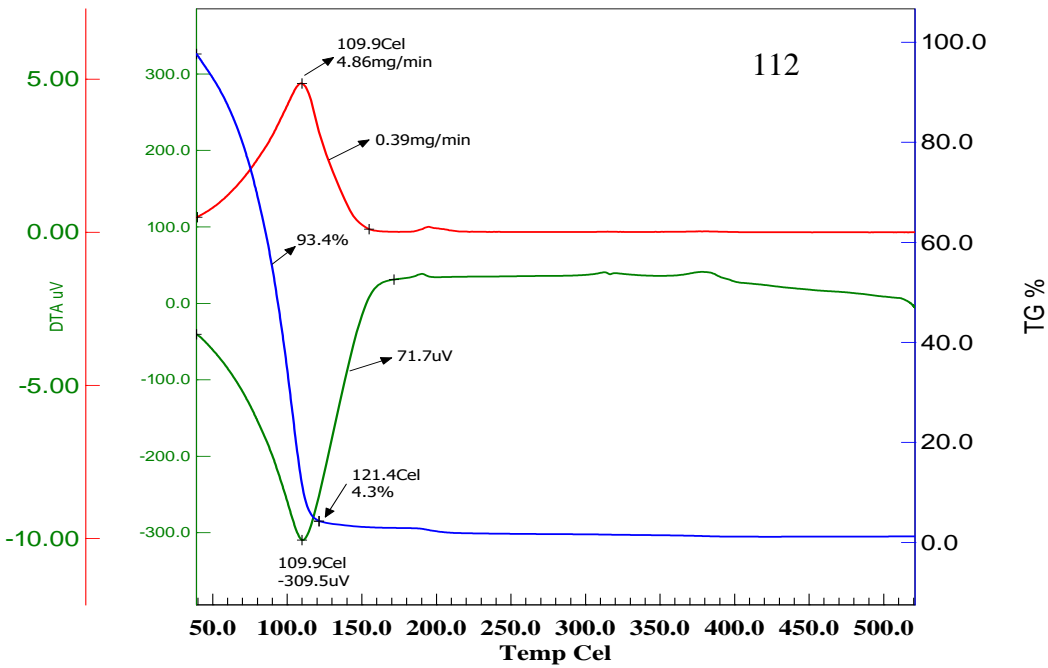


Figure S16. TG-DTA of gel 112.

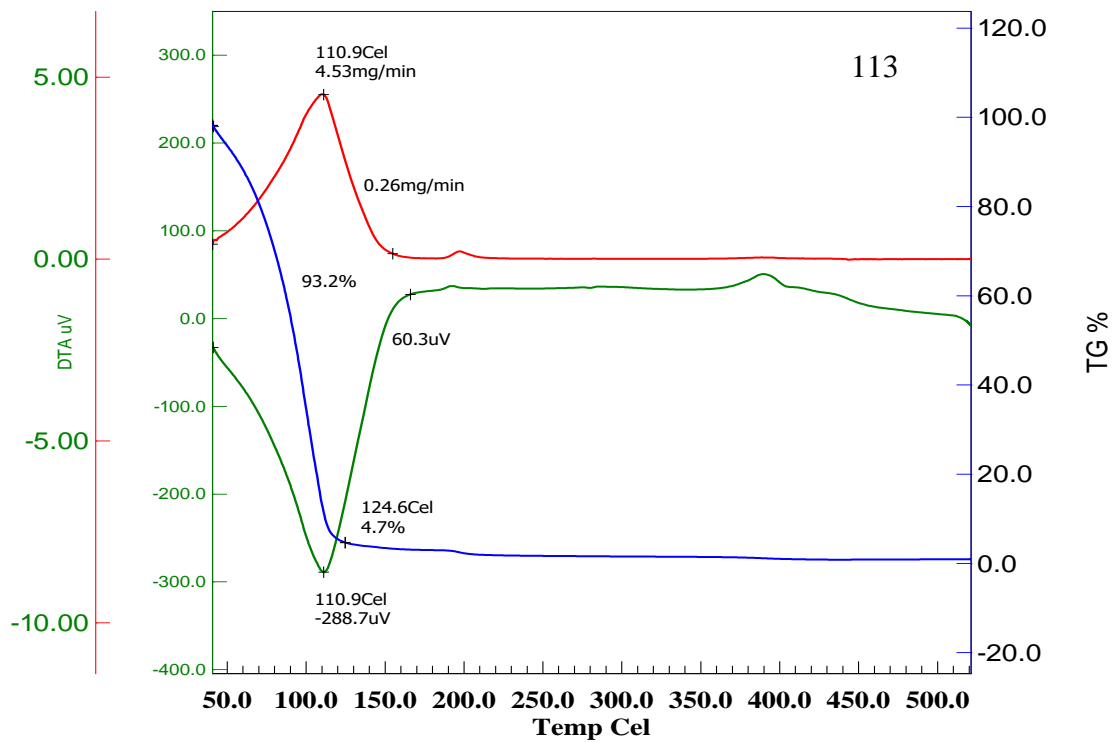


Figure S17. TG-DTA of gel 113.

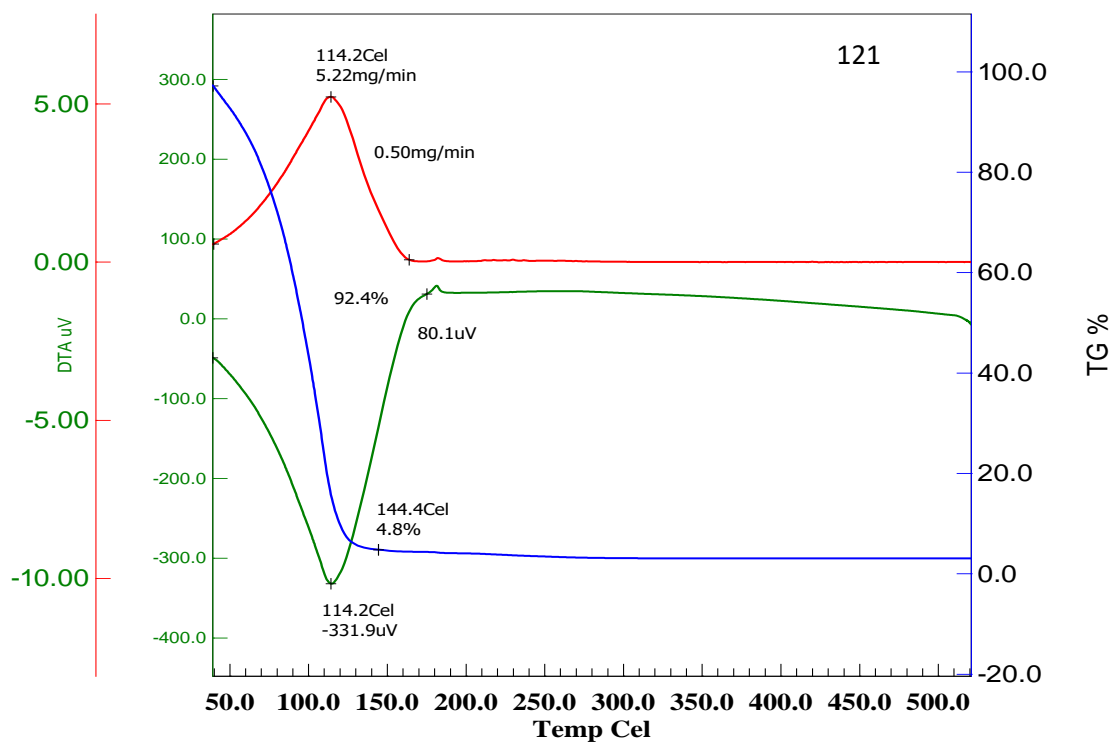


Figure S18. TG-DTA of gel 121.

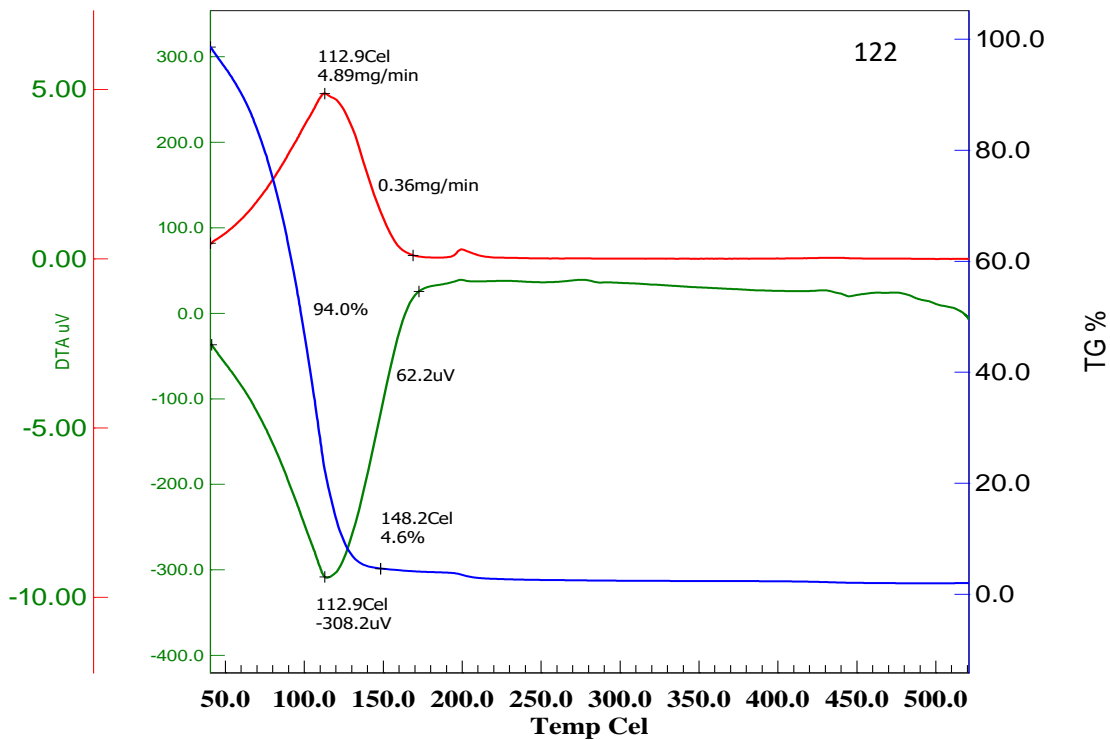


Figure S19. TG-DTA of gel 122.

TG-DTA of xerogels

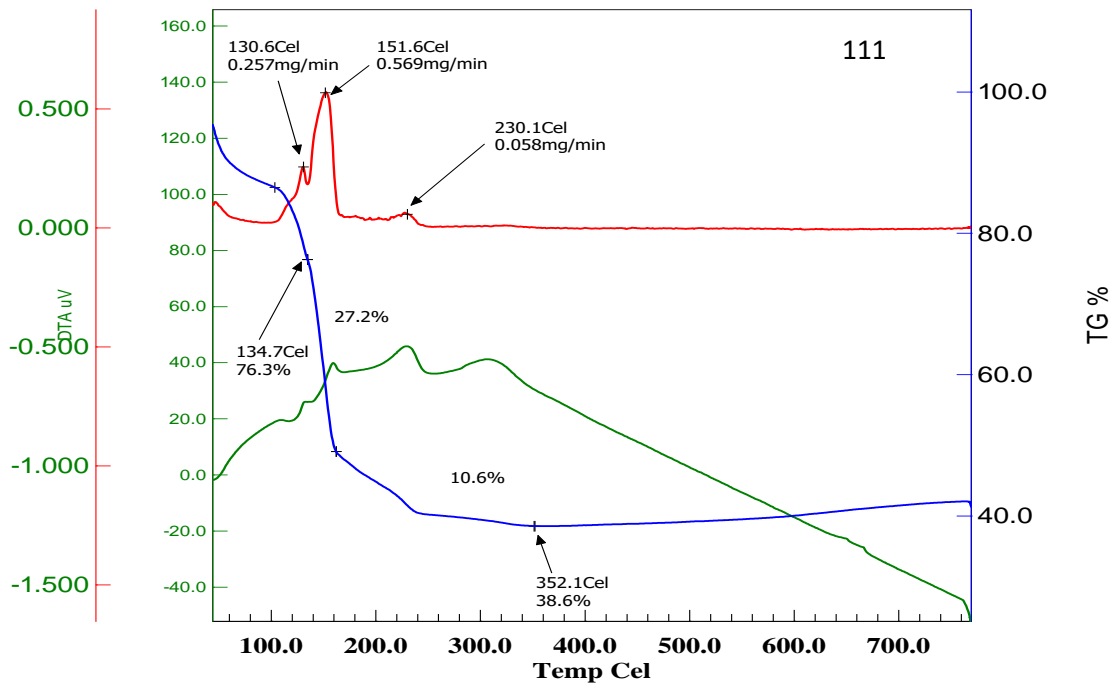


Figure S20. TG-DTA of xerogel 111.

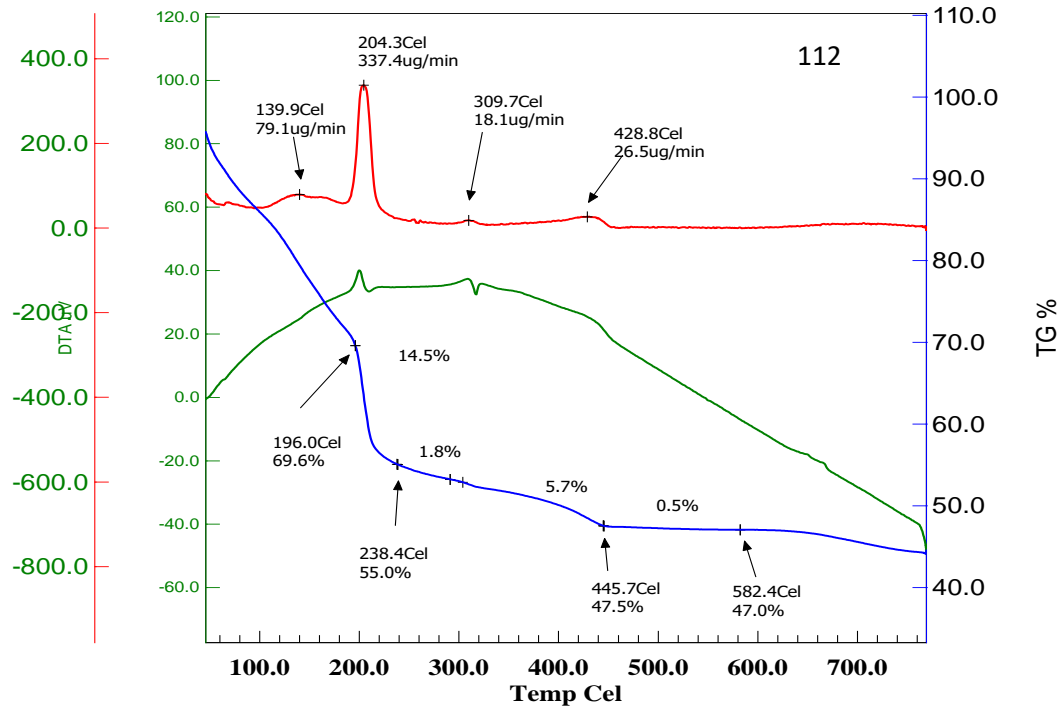


Figure S21. TG-DTA of xerogel 112.

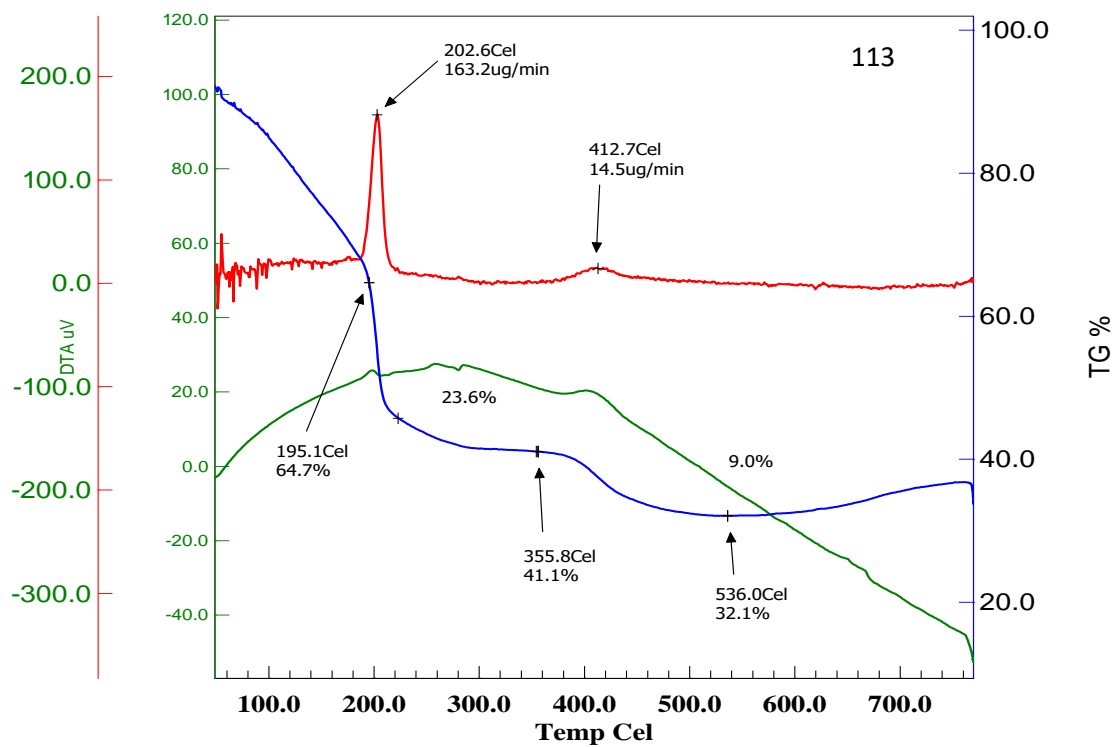


Figure S22. TG-DTA of xerogel 113.

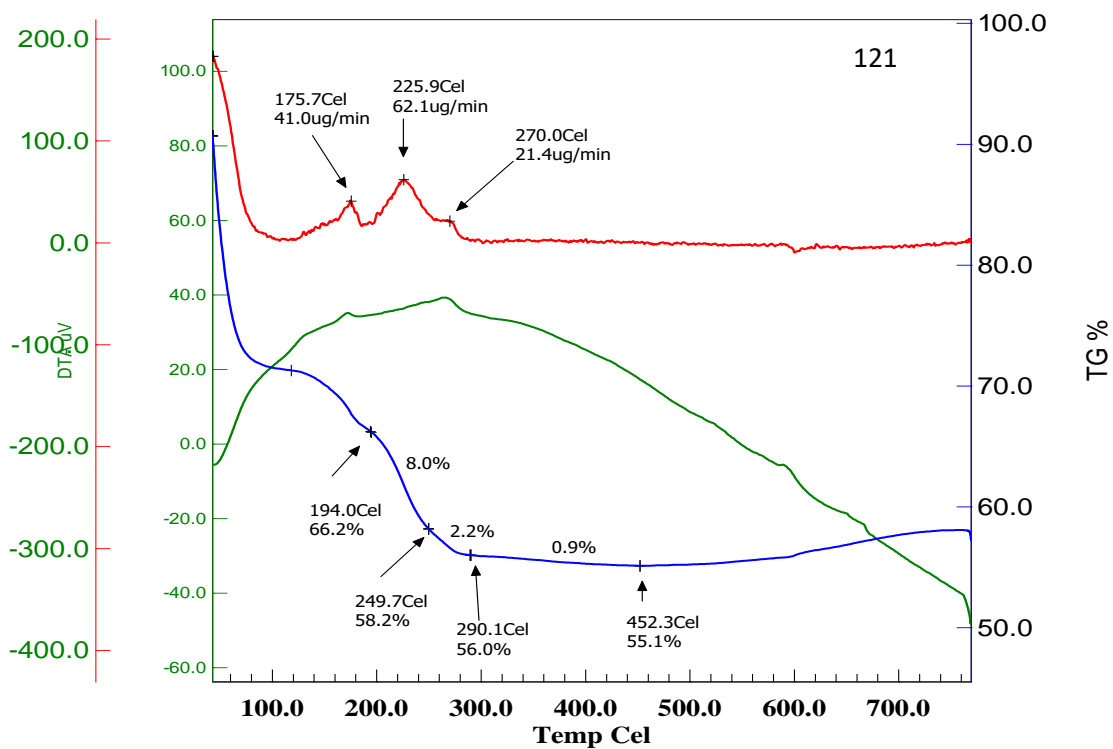


Figure S23. TG-DTA of xerogel 121.

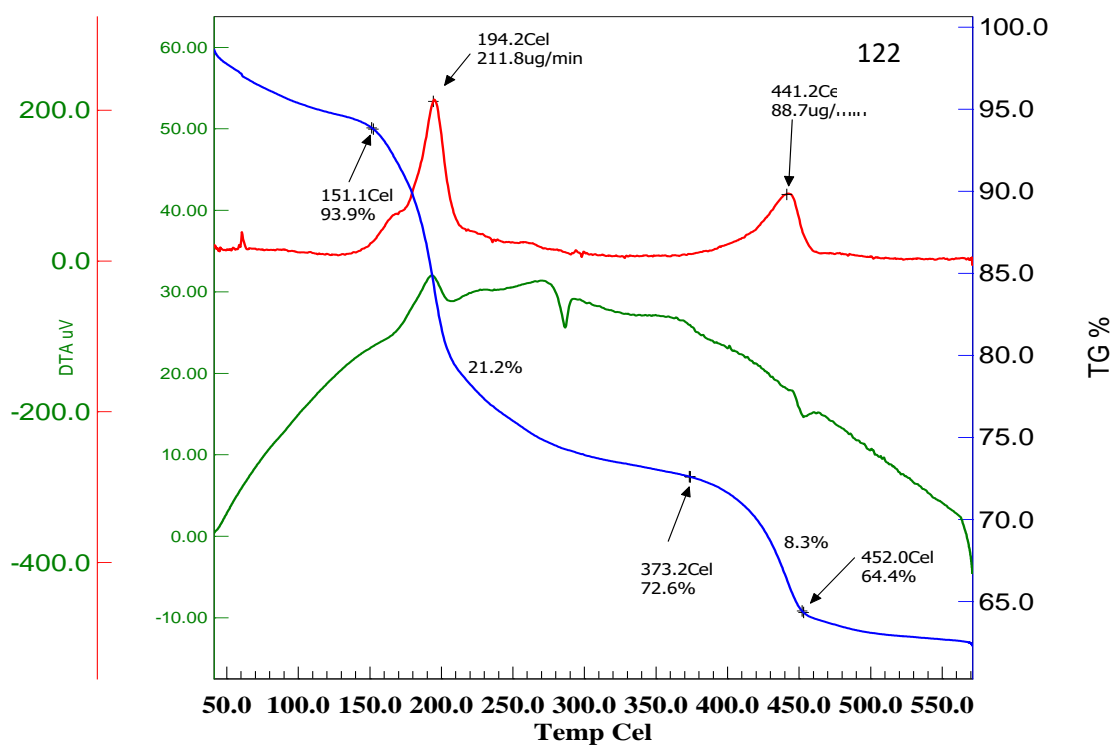


Figure S24. TG-DTA of xerogel 122.

e) Effect of anions in the formation

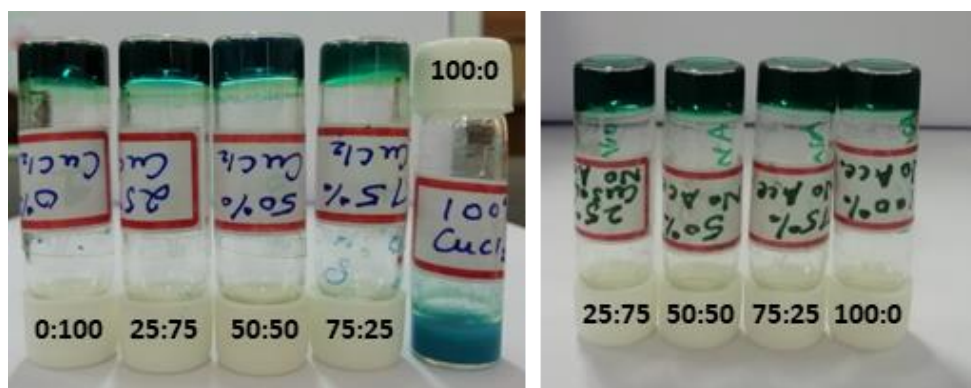


Figure S25. Effect of different ratios of copper chloride : copper acetate (left) and copper sulphate copper acetate(right) on gel formation.

f) Rheological studies of metallogels

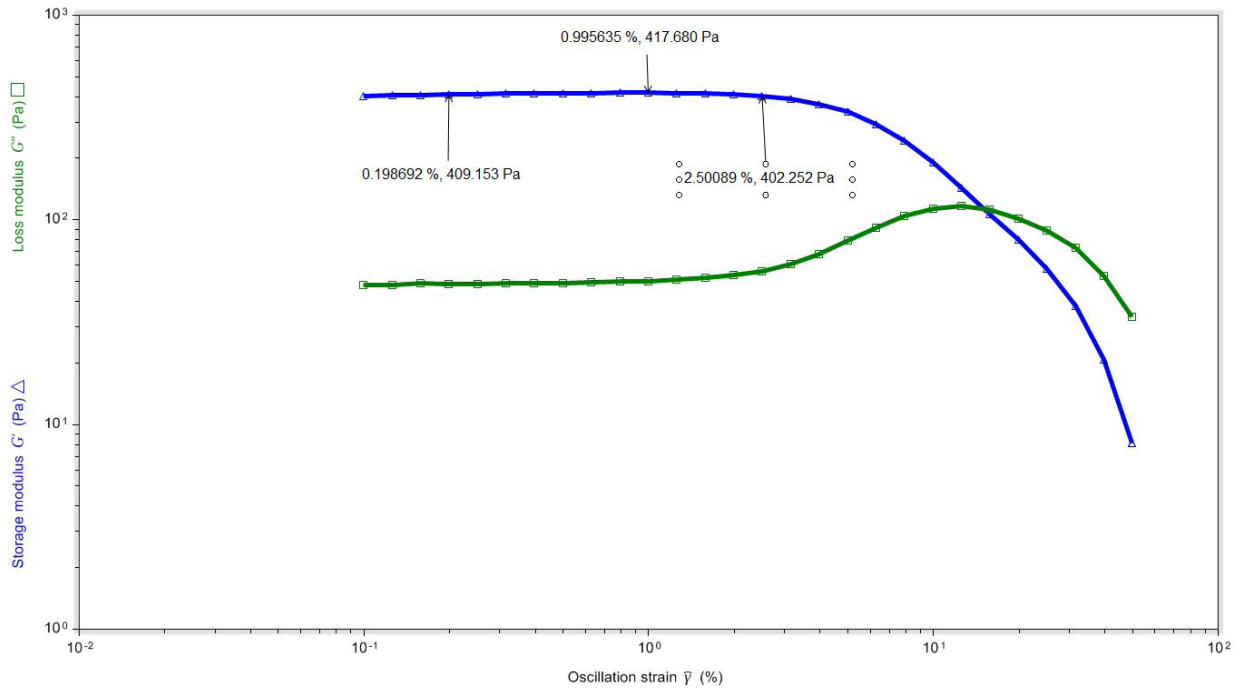


Figure S26: Frequency sweep graph of the gel 121 (Amplitude sweep performed at room temperature @10rad/sec)

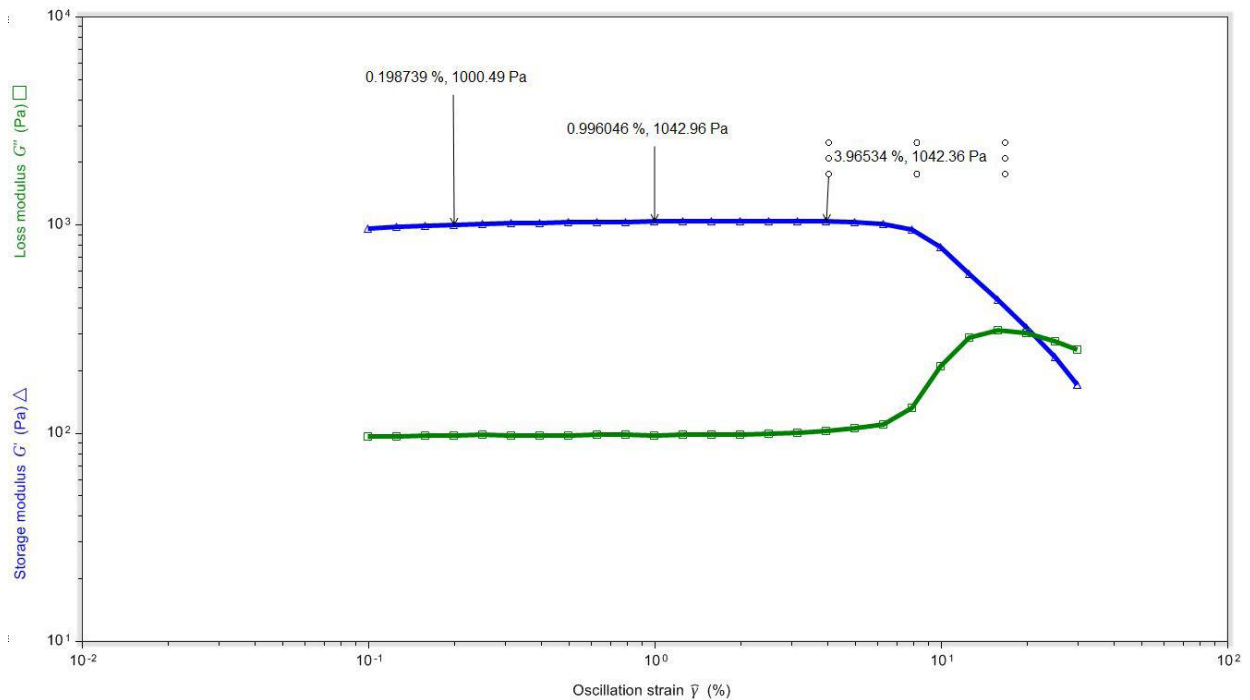


Figure S27: Frequency sweep graph of the gel 122 (Amplitude sweep performed at room temperature @10rad/sec)

g) Polarized microscope images (POM)

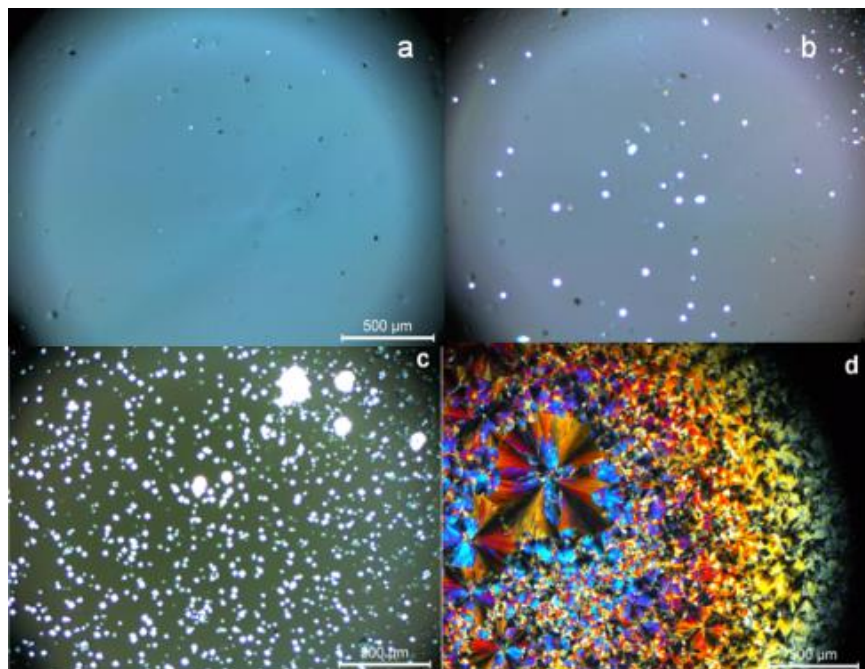


Figure S28. Images [a] to [d] show a gradual change from the isotropic solution to a gel and further to an anisotropic birefringent xerogel.

h) Optimized geometrical parameters involving metal coordination.

Cu-N Distances (Ao)		
R(24,82)	N24-Cu82	2.0083
R(32,82)	N32-Cu82	1.9934
R(62,83)	N62-Cu83	2.0013
R(68,83)	N68-Cu83	1.9924
R(42,84)	N42-Cu84	1.9926
R(48,84)	N48-Cu84	2.0056
Cu-O Distances (Ao)		
R(8,82)	O8-Cu82	2.0807
R(12,82)	O12-Cu82	1.9118
R(11,83)	O11-Cu83	2.0969
R(7,83)	O7-Cu83	1.9193
R(9,84)	O9-Cu84	2.0551
R(10,84)	O10-Cu84	1.9133
Bond angles		
A(8,82,12)	O8-Cu82-O12	84.4064
A(8,82,24)	O8-Cu82-N24	100.9129
A(12,82,32)	O12-Cu82-N32	94.8474
A(24,82,32)	N24-Cu82-N32	82.3473
A(7,83,11)	O7-Cu83-O12	85.4213
A(7,83,68)	O7-Cu83-N68	95.7818
A(11,83,62)	O11-Cu83-N62	97.3579
A(62,83,68)	N62-Cu83-N68	82.3852
A(9,84,10)	O9-Cu84-O10	83.9133
A(9,84,48)	O9-Cu84-N48	98.6515
A(10,84,42)	O10-Cu84-N42	97.0066
A(42,84,48)	N42-Cu84-N48	82.3591
Torsional angles		
L(8,82,32,24,-1)	O8-Cu82-N32-N24 (-1)	183.2601
L(12,82,24,32,-1)	O12-Cu82-N24-N32 (-1)	177.1946
L(7,83,62,68,-1)	O7-Cu83-N62-N68 (-1)	178.1669
L(11,83,68,62,-1)	O11-Cu83-N68-N62 (-1)	179.743
L(9,84,42,48,-1)	O9-Cu84-N42-N48 (-1)	181.0106
L(10,84,48,42,-1)	O10-Cu84-N48-N42 (-1)	179.3657
L(8,82,32,24,-2)	O8-Cu82-N32-N24 (-2)	163.1729
L(12,82,24,32,-2)	O12-Cu82-N24-N32 (-2)	170.8925
L(7,83,62,68,-2)	O7-Cu83-N62-N68 (-2)	188.0659
L(11,83,68,62,-2)	O7-Cu83-N62-N68 (-2)	186.9341
L(9,84,42,48,-2)	O9-Cu84-N42-N48 (-2)	192.5417
L(10,84,48,42,-2)	O10-Cu84-N48-N42 (-2)	189.0303

Table TS1.: Optimized geometrical parameters involving metal coordination.